JMEPEG (2015) 24:4789–4796
DOI: 10.1007/s11665-015-1800-y

1059-9495/$19.00

The Effect of Al_2Cu Precipitate Size on Microstructure and Mechanical Properties of Al-2 wt.%Cu Alloys Fabricated by ARB

B. Azad and E. Borhani

(Submitted April 22, 2015; in revised form November 2, 2015; published online November 18, 2015)

The effect of pre-existing precipitates on microstructure evolution, mechanical properties, and fracture behavior of Al-2 wt.%Cu alloy during accumulative roll-bonding (ARB) process was investigated. Aging treatment was done on Al-2 wt.%Cu alloy in order to produce the nano-particle size precipitates. The microstructure evolution was studied using transmission electron microscope and electron backscattering diffraction (EBSD), and mechanical properties were investigated using tensile test and Vickers micro-hardness measurements. The fine precipitates were formed after the aging process and improved the mechanical properties in the Aged-specimen compared to the solution-treated (ST) specimen. The EBSD analysis showed that the grain size after 6-cycle ARB process has decreased down to 650 and 420 nm for the ST-ARB and the Aged-ARB specimens, respectively. Also, with increasing the number of the ARB cycles, the fraction of HAGBs is increased in both the ST and Aged-specimens. It was found that as the number of cycles increased, the Vickers microhardness value and the yield strength and the tensile strength increased. The scanning electron microscope (SEM) images showed that as the number of the ARB cycles increased, the dimple size became smaller.

Keywords accumulative roll-bonding (ARB) process, Al-2 wt.%Cu alloy, fracture behavior, mechanical properties, microstructure evolution, pre-existing precipitates

1. Introduction

Interest in the processing of bulk ultrafine grained (UFG) materials through the application of severe plastic deformation (SPD) has significantly grown (Ref 1, 2). Several SPD techniques have been designed for achieving high strength metals with minimal changes in the initial sample dimensions. Some SPD techniques, such as equal-channel angular pressing (Ref 3), high pressure torsion (Ref 4), cyclic extrusion compression (Ref 5), and accumulative roll-bonding (ARB) (Ref 6) have been developed. Among these SPD techniques, the ARB process allows to accumulate very large plastic strains into materials without changing the dimensions of the materials by repeating the process of cutting the rolled sheet, stacking them in the initial thickness and roll-bonding the stacked sheets again (Ref 6).

The microstructure evolution, mechanical properties, and texture evolution of ARB-processed alloys have been studied by many researchers (Ref 7-13). However, pre-aging behavior of ARBed specimens has been rarely studied until now. UFG materials which are grain boundaries show unique precipitation behavior (Ref 1, 2, 8-11). One of the limited information about this issue was reported by Borhani et al. (Ref 10), in which the effect of pre-aging on microstructure and mechanical property of Al-0.2 wt.%Sc deformed by ARB process was studied. Their report clearly showed that pre-aging of starting microstructure significantly affects both the microstructure evolution and change in the mechanical properties. Also, Borhani et al. reported microstructural evolution during ARB process of Al-0.2 mass%Sc alloy containing Al_3Sc precipitates in starting structures (Ref 11), and they mentioned after many cycles of the ARB process, the saturated grain size in the Aged-specimens were smaller than that in the ST-specimens (non-precipitates).

Tsuji et al. (Ref 14) reported that the temperature is increased in the SPD process due to large plastic strain and it is reached to 130 °C for 1100 commercial purity aluminum during ARB process. However, Silcock et al. (Ref 15) showed that this increasing of temperature (130 °C) is not sufficient for precipitation in Al-2Cu alloy as the precipitation kinetics is very slow and almost no precipitation occurs at 130 °C for aging up to 10 days. Also, it is reported that only θ' phase precipitates without GP zones at 190 °C in the Al-2 Cu alloy (Ref 15). Murayama et al. reported unusual and interesting precipitation behaviors of two-phase Al-1.7 at.%Cu alloy deformed by equal-channel angular pressing. According to their report, the formation of metastable phases is skipped in aging of the SPD sample (Ref 16). In the present study, the effect of pre-aging process on the microstructure evolution, mechanical properties, and fracture behavior during the ARB process was studied. On the other hand, these properties were investigated in the specimen containing the Al_2Cu precipitates in the starting structure compared to the ST-specimen during the ARB process.

2. Material and Methods

An Al-2 wt.%Cu alloy was prepared as sheets with thickness of 2 mm, width of 60 mm, and length of 200 mm.

B. Azad, Faculty of Metallurgical and Materials Engineering, Semnan University, Semnan, Iran; and **E. Borhani**, Nano-materials Group, Department of Nanotechnology, Semnan University, Semnan, Iran. Contact e-mail: bahramazad1987@gmail.com.

The chemical composition of the used material is as follows (wt.%): 1.96Cu-0.001Mg-0.022Fe-0.004Si-0.001Mn-0.006Cr-0.0001Ti-Al (base). The sheets were solution-treated at 550 °C/6 h and immediately quenched in the water. The solution heat treatment was designed to maximize the solubility of solute elements which are precipitated during subsequent aging. Some of the ST sheets were aged at 190 °C for 30 min, in order to have very fine Al_2Cu precipitates. These two types of the sheets were used as the starting materials for the ARB process. The starting sheets with thickness of 2 mm were first cold-rolled by 50% reduction in the thickness which is named as the first ARB cycle. The 50% rolled sheets of 1 mm thick were cut into two pieces. To prepare the sheets and create a satisfactory bond in the ARB process, the surfaces of the sheets were cleaned by acetone and were roughened by a wire brush and then roll-bonded by 50% reduction in the one pass at room temperature. The same procedures were repeated up to 6 cycles including the first cold-rolling, which corresponded total equivalent strain of 4.8. The ARB process was immediately carried out to avoid for any oxide formation. The ARB process was carried out by two mills with 110 mm diameter rolls having rolling speed of 0.167 m/s. The thermal and mechanical procedures used in this study are schematically shown in Fig. 1.

Sections normal to the transverse direction (TD) of the sheets were used for the microstructural observations. Electron backscattering diffraction (EBSD) analysis was carried out in a scanning electron microscope (SEM) with a field emission type gun (FE-SEM; Philips XL30) operated at 15 kV using a step size of 0.05 μm. The specimens were mechanically polished and then electro-polished in a solution of 30% HNO_3 and 70% CH_3OH before the measurements. The EBSD data were analyzed by orientation imaging microscopy (OIM) software. The software determines the position of all grain-delimiting boundaries, again using the criteria specified by the operator, and calculates several characteristics of each grain, including area, equivalent circle diameter, aspect ratio (of a fitted ellipse), number of neighbors, and internal deformation by lattice rotation. In order to evaluate more accurately, grain size was manually evaluated using the EBSD images by interception method. Interception method was used on the several EBSD images at each cycle and then the mean value of grain size was reported. It should be noted that the grain boundary mapping with a step size of 0.05 μm was used to characterize the samples. The transmission electron microscope (TEM) observations were carried out using Hitachi H-800 operated at 200 kV. Thin foil specimens normal to TD were prepared through mechanical polishing firstly down to approximately 70 μm in the thickness and then electro-polishing in the same solution as that for the EBSD specimens. The tensile test was carried out by a strain rate approximately 8×10^{-3} s^{-1}. The tensile test specimens were machined from the rolled sheets according to the ASTM-E8M standard, oriented along the rolling direction (RD). The mean value of hardness was evaluated by Vickers microhardness with the load of 0.49 N and a loading period of 10 s at room temperature. Finally, the fracture surfaces were studied using SEM micrographs.

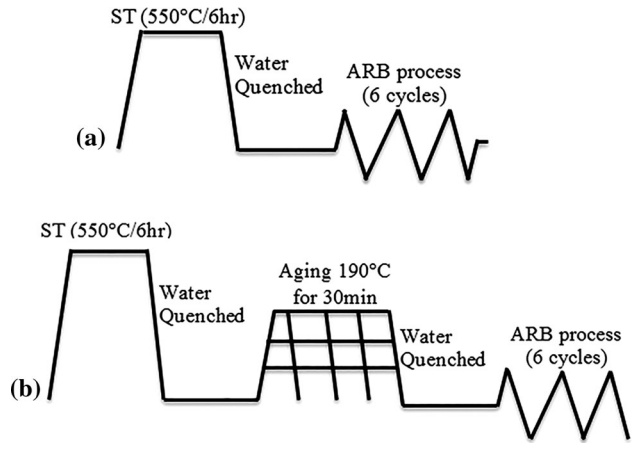

Fig. 1 Schematic illustration of the processes for (a) the ST-ARB and (b) the Aged-ARB specimens

3. Results and Discussion

3.1 Microstructure Evolution

The TEM micrograph of the Aged-specimen before the ARB process is shown in Fig. 2. Because the diffraction spots of Al_2Cu precipitates are very weak, it is difficult to know the orientation of these Al_2Cu precipitates. Therefore, Ashby-Brown contrasts (Ref 17, 18) are used to understand the degree of coherency between a particle and the matrix. The Ashby and Brown contrast consists of spherical strain lines and irregular strain lines. The Ashby and Brown contrast appears around a spherical coherent precipitate in bright-field images. Loss of spherical strain caused by the introduction of interfacial dislocations is detected by the irregularity of the strain lines in the Ashby-Brown contrast. It is well known that the spherical strain lines appear around a spherical coherent precipitate, whereas irregular strain lines appear inside a semi-coherent. As shown in this figure, there are the fine Al_2Cu precipitates having the average precipitates size of 16 nm, after the aging process. Also, the average distance between the precipitates is 33 nm.

Grain boundary maps obtained from EBSD analysis of the ST-ARB and the Aged-ARB specimens after various cycles of the ARB process are shown in Fig. 3. In the boundary map, high-angle grain boundaries (HAGBs) with misorientation angles above 15° are shown as green lines, while low-angle grain boundaries (LAGBs) with misorientation angles between 2° and 15° are shown as red lines. The boundaries with

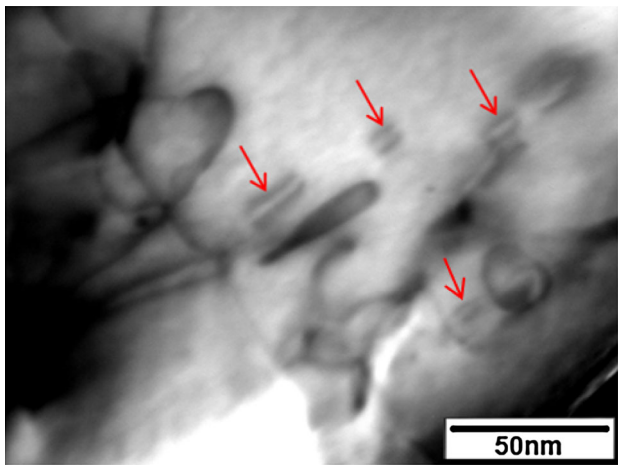

Fig. 2 TEM micrograph of the Aged-specimen before the ARB cycles showing the fine precipitates (indicated by arrows)

misorientation smaller than 2° were omitted in order to remove the inaccuracy due to limited angular resolution in the EBSD measurements. After the 1-cycle and 3-cycle ARB process, corresponding to equivalent strain $\varepsilon = 0.8$ and 2.4, respectively, the microstructures of the matrix are not uniform and consist of two kinds of grain sizes, i.e., the fine grains and the coarse and elongated grains. The fine grains are surrounded by HAGBs while the coarse grains include LAGBs. Both 1-cycle ARB-processed specimens show similar deformation microstructure composed of aligned dislocation boundaries and small amount of HAGBs. It seems that the number of the fine grains surrounded by HAGBs and the amount of LAGBs are both larger in the Aged-ARB specimen than that in the other specimen. After the ARB-6 cycle, corresponding to equivalent strain $\varepsilon = 4.8$, the microstructures are still inhomogeneous. Some regions are relatively included high density of LAGBs while the other regions show elongated UFG structures with high density of HAGBs. It is found that the fraction of HAGBs (f_{HAGBs}) in the Aged-ARB specimen is larger than that of the ST-ARB specimen. This tendency has been also reported by Borhani et al. in Al-Sc alloy (Ref 10). The f_{HAGBs} obtained from the EBSD measurements of the ARBed specimens is given in Fig. 4. As shown in this figure, with increasing the number of the ARB cycles up to 6, the f_{HAGBs} increases and reaches to 13 and 39% in the ST-ARB and the Aged-ARB specimens, respectively. It is agreed that SPD processes and dislocation activity give rise to a change in the microstructure state of HAGBs in metals. Also, it is well known that second-phase particles can increase the rate of dislocation accumulation, and develop local deformation zones containing large local misorientation (Ref 19, 20). This can lead to an increased rate in generation of HAGBs during plastic deformation (Ref 21, 22). The results show that the rate of HAGBs formation is accelerated in the Aged-ARB specimens by the pre-existing precipitates compared to the ST-ARB specimens. On the other hand, the HAGBs evolve with a faster rate in the Aged-ARB specimens compared to the ST-ARB specimens.

Figure 5 shows change in the grain size as a function of the number of the ARB cycles. The grain size was evaluated as the mean spacing of HAGBs along normal direction (ND) by linear intercept method in the EBSD boundary maps. The grain size of the specimens decreases with increasing the number of the ARB cycles and reaches to 650 and 420 nm for the ST-ARB and Aged-ARB specimens after applying the total equivalent strain of 4.8, respectively. From the results of the EBSD measurements, it is concluded that grain refinement by SPD process is accelerated by pre-existing precipitates. Here, it is noteworthy that the grain size of the Aged-ARB specimen is smaller than that of the ST-ARB specimen. This acceleration is presumably attributed to the inhibition of dislocation motion by the precipitates (Ref 10, 11). It is expected that the accumulation of dislocations is accelerated because the dislocation motion is inhibited by the precipitates during the ARB process. These results are consistent with the previous studies on ARB process (Ref 10, 11, 23). The results show that the presence of second-phase particles could potentially have a significant effect on the formation of the UFG structures during the ARB process. On the other hand, existence of the fine precipitates in the starting material greatly accelerates the microstructure refinement. Therefore, the formation of the UFG microstructure is accelerated when the starting microstructure involved fine precipitates. Also, the fine precipitates can inhibit the grain boundary migration during the ARB process that it causes the

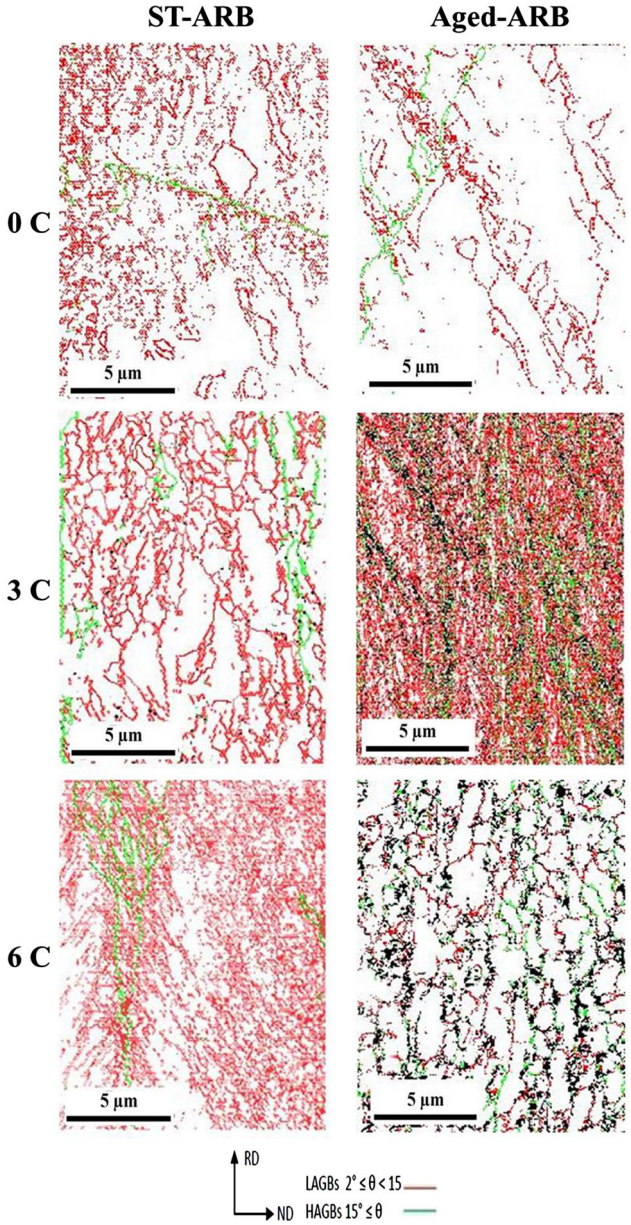

Fig. 3 Grain boundary maps obtained from EBSD measurement for the ST-ARB and the Aged-ARB specimens by various cycles at room temperature

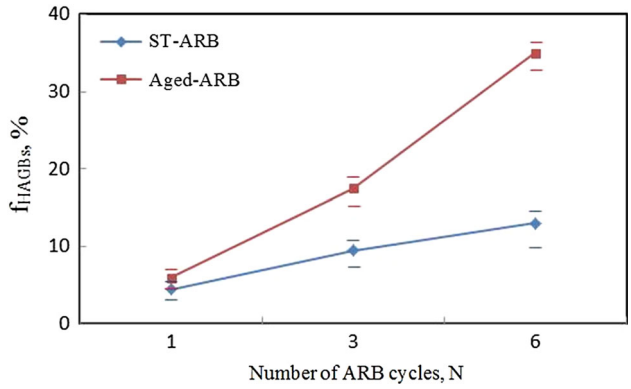

Fig. 4 The fraction of HAGBs of the ARBed specimens

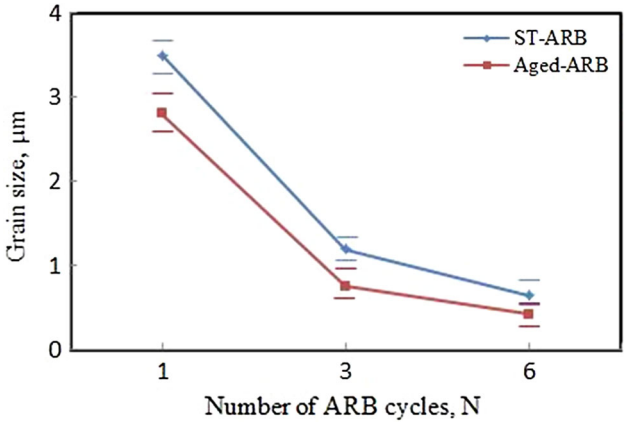

Fig. 5 Change in the grain size as a function of the number of the ARB cycles

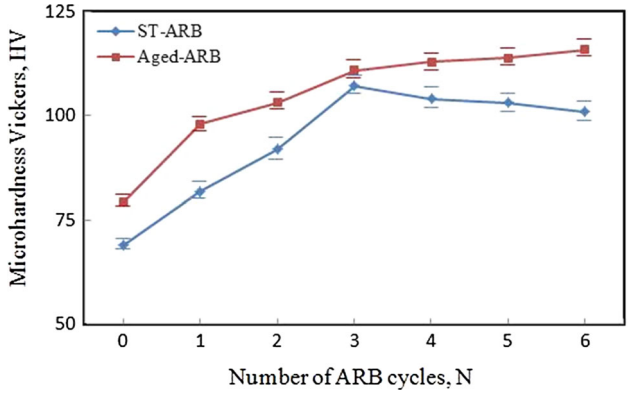

Fig. 6 Change in the Vickers microhardness value of the specimens as a function of the number of the ARB cycles

smaller grain size in the Aged-ARB specimen compared to the ST-ARB specimen (Ref 11). However, we should note that the UFG structures in the ARB-processed specimens are not controlled only by the grain growth but are the results of grain subdivision during heavy plastic deformation (Ref 11).

3.2 Mechanical Properties

Figure 6 shows the Vickers microhardness value of the ST-ARB and the Aged-ARB specimens. The Vickers microhardness value of the ST-ARB and the Aged-ARB specimens is 69 HV and 79 HV before the ARB process (0-cycle ARB), respectively. One of the reasons for higher hardness in the Aged-ARB specimen can be related to the pre-existing precipitates. Borhani et al. reported that hardness of Aged-ARB specimens is higher than that of the ST-ARB specimen (Ref 10). This issue is clearly seen in the present study. ARB itself causes an increasing of hardness, however, the additional hardness is resulted by pre-existing precipitates in the Aged-ARB specimens. In addition, the stress fields around coherent precipitates can increase the hardness (Ref 24). The Vickers microhardness value of the ST-ARB specimen increases to 107 HV in 3-cycle ARB process, and slightly decreases with further ARB cycles and reaches to 101 HV after 6-cycle ARB process. On the other hand, the Vickers microhardness value of the Aged-ARB specimen increases with increasing the number of the ARB cycles and reaches to 116 HV after 6-cycle ARB process. As can be seen, the rate of increase of the hardness decreases after 3-cycle ARB process. By continuing ARB cycles, applied large strains may cause dissolution of the pre-existing precipitates (Ref 10, 11), therefore, the pre-existing precipitates have a powerful effect on the microhardness value at relatively low strains.

Stress-strain curves of the ARB-processed specimens obtained from the tensile tests are given in Fig. 7. It is shown that the ST-ARB and the Aged-ARB specimens have different tendencies in the change of mechanical properties during the ARB process. Figure 8 shows the results of the tensile test after various cycles of the ARB process. As shown in Fig. 8(a), the yield strength of the ST-ARB specimen increases with increasing the number of the ARB cycles monotonously up to 3-cycle ARB process, and then slightly decreases with further ARB cycles. The yield strength of the ST-ARB specimen is 55 MPa before ARB process and reaches to 203 MPa after 6-cycle ARB process. On the other hand, the yield strength of the Aged-ARB specimen increases with increasing the number of the ARB cycles and reaches to 228 MPa after 6-cycle ARB process. As can be seen in Fig. 8(b), the tensile strength values of the ST-ARB and the Aged-ARB specimens are 98 MPa and 122 MPa before ARB process, respectively. The tensile strength of the Aged-ARB specimen is higher than that in the ST-ARB specimen, which is almost the same as that in the yield strength. The difference of the yield strength and the tensile strength between the ST-specimen and the Aged-specimen before the ARB process can be due to the existence of precipitates after the aging process. The tensile strength of the ST-ARB specimen increases with increasing the number of the ARB cycles, and keeps nearly a constant value after 3-cycle ARB process. On the other hand, the tensile strength of the Aged-ARB specimen increases with increasing the number of the ARB cycles. Here, it is noteworthy that the effect of the pre-existing precipitates on the yield strength and the tensile strength is more effective in the initial cycles that can be related to dissolution of the pre-existing precipitates due to applying the large strains in the higher cycles of the ARB process. The dissolution of second phase occurring in SPD process is an important phenomenon of phase transformation. It is shown that the ST-ARB and the Aged-ARB specimens have different mechanical properties during the ARB process. The results of tensile test corresponded well with the change in the hardness during the ARB process. Figure 8(a) and (b) clearly show that simultaneous effect of pre-existing precipitates in the starting structure and ARB process on the mechanical properties is more effective than only applying the ARB itself.

The mechanical properties can be calculated based on strengthening mechanisms, i.e., grain boundary strengthening and precipitation strengthening. The two kinds of deformation mechanism observed in materials containing particles are Orowan mechanism (Ref 25) and cut-through mechanism (Ref 25). According to these mechanisms and the critical size of Al_2Cu precipitates reported by Hu et al. (Ref 26), Orowan mechanism should work in the Aged-specimen at least in the initial cycles, because the precipitates size is larger than the critical size of Al_2Cu precipitate. It should be noted that based on Orowan and cut-through mechanisms, the size and volume fraction of the precipitates are the important factors and they affect the mechanical properties. This has been accepted that as

plastic strain increases during ARB process, volume fraction of precipitates decreases (Ref 10, 11). Accordingly, the rate of increase of the strength due to the pre-existing precipitates is reduced with further ARB cycles. This can be related to the influence of high plastic strains on the pre-existing precipitate during the ARB process. This issue can be seen in Fig. 8.

As previously mentioned by other researchers (Ref 10, 11, 27, 28), the precipitates may be fragmented to smaller size or dissolved into the matrix due to strong shear induced by SPD process. Therefore, as previously discussed, it can be concluded that the pre-existing precipitates are more effective on the mechanical properties in the initial cycles corresponding to the low strains. Also, the mechanical properties are correlated to grain boundary strengthening. The increase in the proof stress due to the grain refinement obtained from Hall-Petch equation (Ref 1), $\Delta\sigma_{gb}\left(=kd_t^{-1/2}\right)$, is shown in Fig. 9, where k is a constant and d_t is mean grain size. Various yield strength obtained from the stress-strain curves were plotted against the square root of the mean grain sizes ($d_t^{-1/2}$). The k calculated from the extrapolated curves is 75 Mpa $\mu m^{1/2}$. According to the Hall-Petch equation, the yield strength is dependent on the reciprocal of square root of the grain size. Also, it becomes clear that the grain boundary strengthening of the specimens increases with decreasing the grain size in both ST-ARB and Aged-ARB specimens. It should be noted that the grain boundaries greatly affect the mechanical properties as they can impede the movement of dislocations (Ref 29). The grains have different orientations, therefore, dislocation requires more energy to move into the adjacent grain (Ref 30). However, this grain boundary strengthening value, as shown in Fig. 9, is higher in the Aged-ARB specimen compared to the ST-ARB specimen, since the grain refinement is accelerated in the Aged-ARB specimen due to pre-existing precipitates (Ref 10, 11, 23), as discussed in Fig. 5.

The total elongation and the uniform elongation of the specimens are shown in Fig. 8(c) and (d) after various cycles of the ARB process, respectively. Before the ARB process, the total elongation and the uniform elongation of the ST-specimen are larger than those of the Aged-specimen. This indicates the pre-existing precipitates inhibit the tensile elongation. By 1-cycle ARB process, the total elongation and the uniform elongation of the ST-ARB and the Aged-ARB specimens significantly decrease. The total elongation of the ST-ARB specimens decreases from 62 to 18.5%, and the uniform elongation decreases from 41 to 3%. On the other hand, the total elongation of the Aged-ARB specimen decreases from 45 to 16.5%, and the uniform elongation decreases from 19% to less than 3%. As can be seen in these figures, the change in the

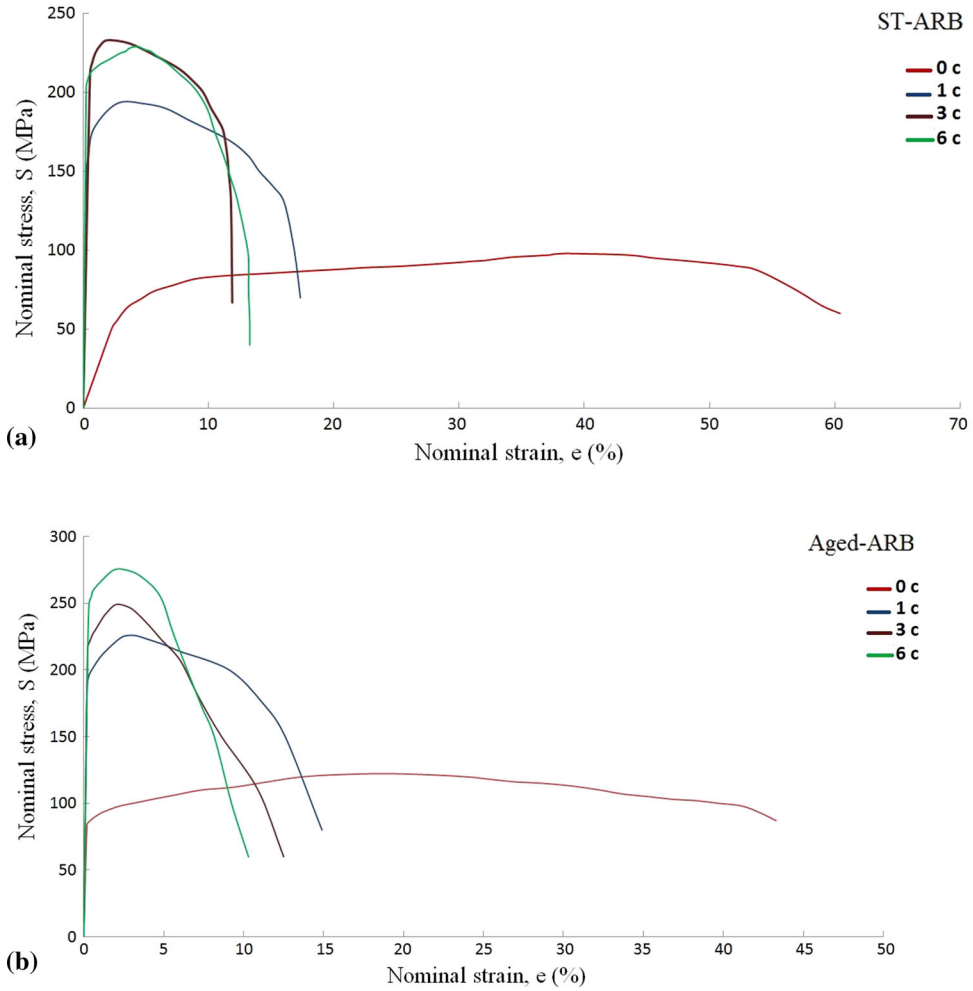

Fig. 7 Tensile stress-strain curves of (a) ST-ARB and (b) Aged-ARB specimens

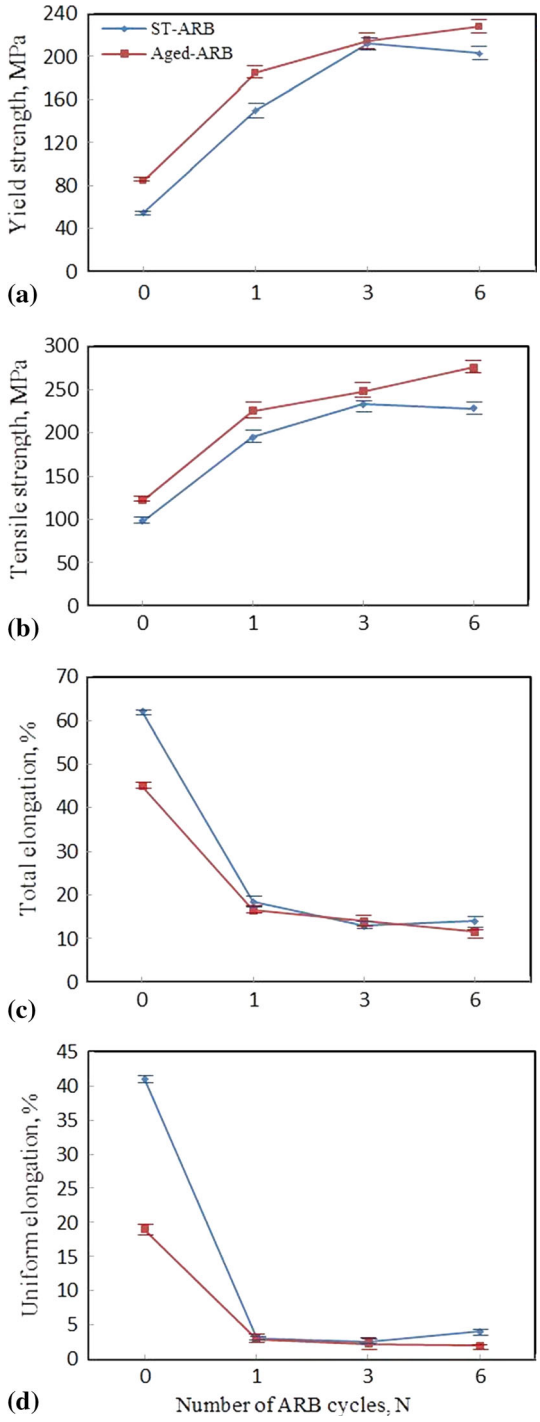

Fig. 8 Mechanical properties of the specimens after various cycles of the ARB process, (a) Yield strength, (b) Tensile strength, (c) Total elongation, and (d) Uniform elongation

elongation of the Aged-ARB specimen is smaller than that in the ST-ARB specimen. By continuing the process in the ST-ARB specimen up to the final cycles, the total elongation nearly shows a constant value, and the uniform elongation gradually increases. On the other hand, by continuing the process in the Aged-ARB specimen up to the final cycles, the total elongation and the uniform elongation decrease slightly. It can be concluded from Fig. 8, although the pre-aging process has a great effect on improving the mechanical properties, but the

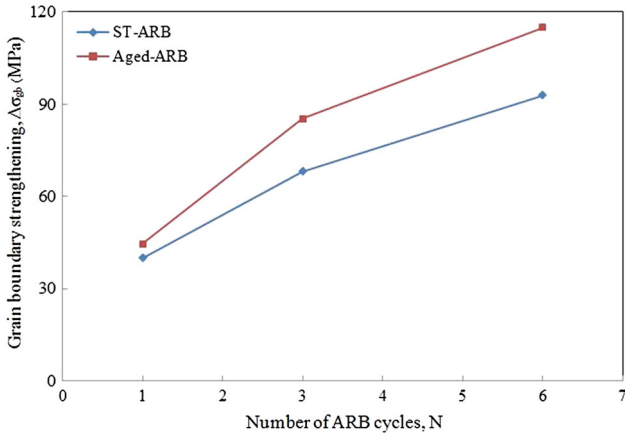

Fig. 9 Flow stress increment from grain size as a function of the number of the ARB cycles

existence of the Al_2Cu precipitates decreases the total and uniform elongation in the Aged-specimen before the ARB process.

3.3 Fractography

Types of fracture can be roughly divided into two categories, which are brittle and ductile fractures (Ref 31, 32). Ductile and brittle describes the amount of macroscopic plastic deformation that precedes fracture (Ref 31). Also, type of fractures can be described by transgranular fracture and intergranular fracture (Ref 31). Transgranular cleavage fracture is usually associated with defects such as cracks, porosity, inclusions, or second-phase particles in which dislocations movement is obstructed (Ref 31). The fracture surfaces of the specimens after various cycles of the ARB process are shown in Fig. 10. As shown at 0-cycle ARB, the dimples indicate the micro-void coalescence (MVC) mechanism of ductile fracture before the ARB process. The shape of the dimples indicates the type of loading the component has experienced during fracture, and the orientation of the dimples reveals the direction of crack extension. Ductile fractures almost have a gray fibrous appearance and equiaxed or hemispheroidal dimples which is clearly seen before the ARB process (Ref 31-33). Different sizes of the dimples are found in the specimens and the sizes of dimples in the ST-ARB specimen are larger than that of the Aged-ARB specimen. This result shows that the ST-specimen and the Aged-specimen have different behaviors in the fracture due to the different starting microstructures. Also, the presence of the small second-phase particles causes the formation of pockets of shallow dimples and microscopic voids of varying sizes (Ref 34). From the tensile test at 0-cycle ARB, the total elongation and the uniform elongation of the ST-ARB specimen are higher compared to the Aged-ARB specimen that it can be related to the larger and deeper dimples in the ST-ARB specimen. As shown in Fig. 10, the size of the dimples significantly decreases with increasing the number of the ARB cycles. By continuing the process, the samples also show a ductile fracture with the dimples but these dimples are not as deep as those in the initial cycle. Also, with increasing the number of the ARB cycles, it can be said that the cleavage facets and the river lines, or the stress lines are steps between

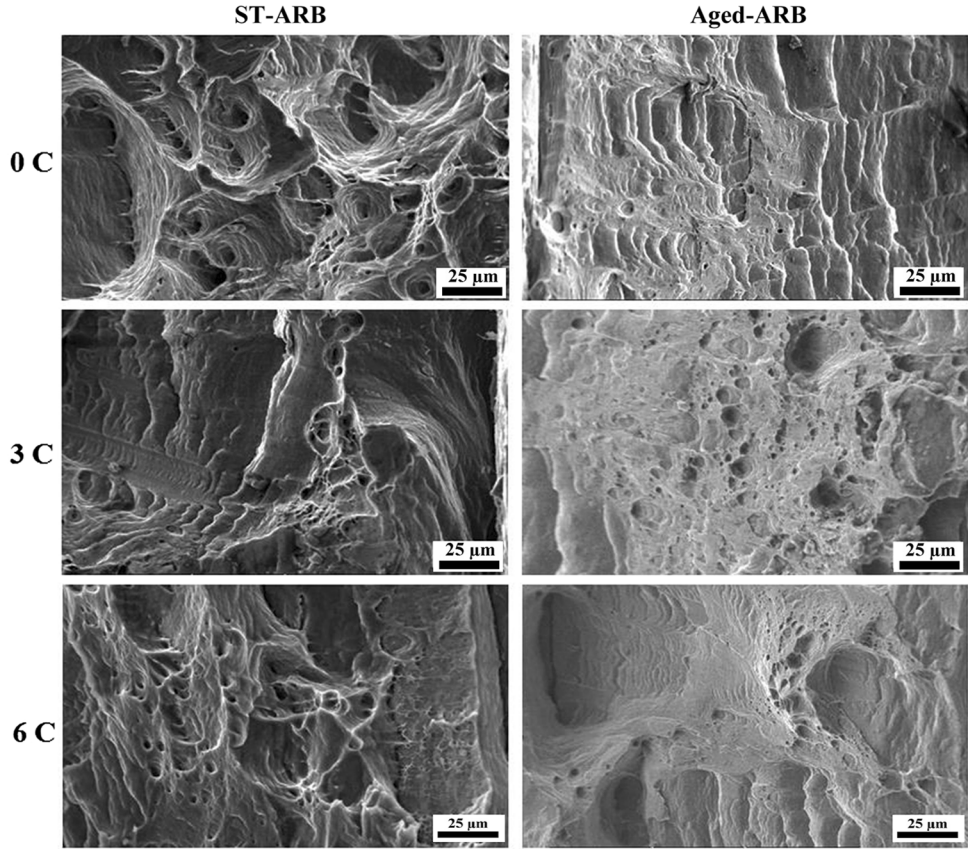

Fig. 10 Fracture surfaces of the ST-ARB and the Aged-ARB specimens after tensile test at various cycles of the ARB process

cleavage or parallel planes, which are always converged in the direction of local crack propagation (Ref 31, 33).

4. Conclusion

The effect of pre-existing precipitates on microstructure evolution, mechanical properties, and fracture behavior was investigated during the ARB process up to 6 cycles. The main results are summarized as follows:

(1) In the Aged-specimen were formed very fine precipitates after the aging process. The specimens containing very fine precipitates had the potential to significantly improve the grain refinement and the mechanical properties. With increasing the number of the ARB cycles, the f_{HAGBs} increased in both the specimens. The f_{HAGBs} in the Aged-ARB specimen was larger than that of the ST-ARB specimen. On the other hand, the rate of the HAGBs formation and the grain refinement were accelerated by the pre-existing precipitates. After 6-cycle ARB process, the mean grain size of the Aged-ARB specimen was smaller compared to the ST-ARB specimen and reached to 650 and 420 nm for the ST-ARB and the Aged-ARB specimens, respectively.

(2) The value of Vickers microhardness value of the Aged-ARB specimen was higher than that of the ST-ARB specimen due to the pre-existing precipitates in the Aged-ARB specimen. The Vickers microhardness value of the Aged-ARB specimen increased with increasing the number of the ARB cycles, while the ST-ARB specimen showed slight softening after 3-cycle ARB process. The results of the tensile test corresponded well with the change in the hardness during the ARB process. The yield strength and the tensile strength of the ST-ARB specimen increased with increasing the number of the ARB cycles up to 3 cycles. After 3-cycle ARB process, the yield strength decreased slightly, while, the tensile strength of the ST-ARB increased up to 3-cycle ARB process and showed a nearly constant value up to 6-cycle ARB process. On the other hand, the yield strength and the tensile strength of the Aged-ARB specimen increased with increasing the number of the ARB cycles. The elongation of the specimens significantly decreased after the ARB process. The change in the elongation of the Aged-ARB specimen is smaller than that in the ST-ARB specimen.

(3) From SEM images, the size of dimples significantly decreased with increasing the number of the ARB cycles. By continuing the process, the samples also showed a ductile fracture with the dimples but these dimples were not as deep as those in the initial cycle. Also, with increasing the number of the ARB cycles, it was seen the cleavage facets and the river lines, that the river lines or the stress lines are steps between cleavage or parallel planes, which are always converged in the direction of local crack propagation.

References

1. A. Azushima, R. Kopp, A. Korhonen, D.Y. Yang, F. Micari, G.D. Lahoti, P. Groche, J. Yanagimoto, N. Tsuji, A. Rosochowski, and A. Yanagida, Severe Plastic Deformation (SPD) Processes for Metals, *Manuf. Technol.*, 2008, **57**, p 716–735
2. R.B. Figueiredo and T.G. Langdon, Using Severe Plastic Deformation for the Processing of Advanced Engineering Materials, *Mater. Trans.*, 2009, **50**, p 1613–1619
3. R.Z. Valiev and T.G. Langdon, Principles of Equal-Channel Angular Pressing as a Processing Tool for Grain Refinement, *Prog. Mater. Sci.*, 2006, **51**, p 881–981
4. R.Z. Valiev, R.K. Islamgaliev, and I.V. Alexandrov, Bulk Nanostructured Materials from Severe Plastic Deformation, *Prog. Mater. Sci.*, 2000, **45**, p 103–189
5. M. Richert, Q. Liu, and N. Hansen, Microstructural Evolution Over a Large Strain Range in Aluminum Deformed by Cyclic-Extrusion–Compression, *Mater. Sci. Eng. A*, 1999, **260**, p 275–283
6. Y. Saito, H. Utsunomiya, N. Tsuji, and T. Sakai, Novel Ultra-high Straining Process for Bulk Materials-Development of the Accumulative Roll-Bonding (ARB) Process, *Acta Mater.*, 1999, **47**, p 579–583
7. E. Borhani, H. Jafarian, A. Shibata, and N. Tsuji, Texture Evolution in Al-0.2 mass% Sc Alloy during ARB Process and Subsequent Annealing, *Mater. Trans.*, 2012, **53**, p 1863–1869
8. P. Hidalgo-Manrique, C.M. Cepeda-Jiménez, A. Orozco-Caballero, O.A. Ruano, and F. Carreño, Evolution of the Microstructure, Texture and Creep Properties of the 7075 Aluminum Alloy During Hot Accumulative Roll Bonding, *Mater. Sci. Eng. A*, 2014, **606**, p 434–442
9. E. Borhani, H. Jafarian, H. Adachi, D. Terada, and N. Tsuji, Annealing Behavior of Solution Treated and Aged Al-0.2wt% Sc Deformed by ARB, *Mater. Sci. Forum.*, 2010, **667**, p 211–216
10. E. Borhani, H. Jafarian, T. Sato, D. Terada, N. Miyajima, and N. Tsuji, *Proceedings of 12th International Conference on Aluminum Alloys* (Japan), 2010, p 2168
11. E. Borhani, H. Jafarian, D. Terada, H. Adachi, and N. Tsuji, Microstructural Evolution During ARB Process of Al-0.2 mass% Sc Alloy Containing Al_3Sc Precipitates in Starting Structures, *Mater. Trans.*, 2011, **53**, p 72–80
12. H. Pirgazi, A. Akbarzadeh, R. Petrov, and L. Kestens, Microstructure Evolution and Mechanical Properties of AA1100 Aluminum Sheet Processed by Accumulative Roll Bonding, *Mater. Sci. Eng. A*, 2008, **497**, p 132–138
13. S.H. Lee, Y. Saito, T. Sakai, and H. Utsunomiya, Microstructure and Mechanical Properties 6061 Aluminum Alloy Processed by Accumulative Roll Bonding, *Mater. Sci. Eng. A*, 2002, **325**, p 228–235
14. N. Tsuji, T. Toyoda, Y. Minamino, Y. Koizumi, T. Yamane, M. Komatsu, and M. Kiritani, Microstructural Change of Ultrafine-Grained Aluminum During High-Speed Plastic Deformation, *Mater. Sci. Eng. A*, 2003, **350**, p 108–116
15. J.M. Silcock, T.J. Heal, and H.K. Hardy, Structural Aging Characteristics of Binary Aluminium–Copper Alloys. *J. Inst. Met.* 1953–1954, **82**, p 239–248
16. M. Murayama, Z. Horita, and K. Hono, Microstructure of Two-Phase Al-1.7 at% Cu Alloy Deformed by Equal-Channel Angular Pressing, *Acta Mater.*, 2001, **49**, p 21–29
17. X. Huang, N. Tsuji, N. Hansen, and Y. Minamino, Microstructural Evolution During Accumulative Roll-Bonding of Commercial Purity Aluminum, *Mater. Sci. Eng. A*, 2003, **340**, p 265–271
18. B.G. Clark, I.M. Robertson, L.M. Dougherty, D.C. Ahn, and P. Sofronis, High-Temperature Dislocation-Precipitate Interactions in Al Alloys: An In Situ Transmission Electron Microscopy Deformation Study, *Mater. Res.*, 2005, **20**, p 1792–1801
19. F.J. Humphreys and P.B. Hirsch, Work-Hardening and Recovery of Dispersion Hardened Alloys, *Philos. Mag.*, 1976, **34**, p 373–390
20. F.J. Humphreys, Local Lattice Rotations at Second Phase Particles in Deformed Metals, *Acta Metal.*, 1979, **27**, p 1801–1814
21. P.J. Apps, J.R. Bowen, P.B. Prangnell, Nanomaterials by Severe Plastic Deformation-NANSPD2, M. Zehetbauer, R.Z. Valiev, Eds., Vienna, Austria, 2002, p 138
22. P.J. Apps, J.R. Bowen, and P.B. Prangnell, The Effect of Coarse Second-Phase Particles on the Rate of Grain Refinement During Severe Deformation Processing, *Acta Mater.*, 2003, **51**, p 2811–2822
23. B.K. Min, H.W. Kim, and S.B. Kang, Effect of Al_3Sc Precipitate on the Microstructural Evolution During Accumulative Roll Bonding in Al–0.2 wt.% Sc Alloy, *J. Mater. Process. Technol.*, 2005, **162–163**, p 355–361
24. S.G. Jia, M.S. Zheng, P. Liu, F.Z. Ren, B.H. Tian, G.S. Zhou, and H.F. Lou, Aging Properties Studies in a Cu–Ag–Cr Alloy, *Mater. Sci. Eng. A*, 2006, **419**, p 8–11
25. R.E. Smallman and R.J. Bishop, *Metals and Materials: Science, Processes, Applications*, Butterworth-Heinemann, Oxford, 1995
26. S.Y. Hu, M.I. Baskes, M. Stan, and L.Q. Chen, Atomistic calculations of interfacial energies, nucleus shape and size of θ′ precipitates in Al–Cu alloys, *Acta Mater.*, 2006, **54**, p 4699–4707
27. I. Gutierrez-Urrutia, M.A. Mu~noz-Morris, and D.G. Morris, The Effect of Coarse Second-Phase Particles and Fine Precipitates on Microstructure Refinement and Mechanical Properties of Severely Deformed Al Alloy, *Mater. Sci. Eng. A*, 2005, **394**, p 399–410
28. Z. Horita, K. Oh-ishi, and K. Kaneko, Microstructure control using severe plastic deformation, *Sci. Tech. Adv. Mater.*, 2006, **7**, p 649–654
29. J. Rosler, H. Harders, and M. Baker, *Mechanical Behaviour of Engineering Materials: Metals, Ceramics, Polymers and Composites*, Springer, Berlin, 2007
30. J. Wang, I.J. Beyerlein, A. Misra, S.M. Valone, and T.C. Germann, Atomistic Modeling of Dislocation-Interface Interaction, *3rd International Conference on Heterogeneous Material Mechanics*, May 22–26 (Shanghai, China), 2011
31. ASM, *ASM Metals Handbook Fractography*, Vol 12, ASM, Metals Park, 1987
32. R.W. Hertzberg, *Deformation and Fracture Mechanics of Engineering Materials*, 3rd ed., John Wiley & Sons Inc., Singapore, 1989
33. B. Azad, E. Borhani, and H.R. Mohammadian Semnani, Fracture Behavior of Al-0.2wt%Zr Alloy Processed by Accumulative Roll Bonding (ARB) Process, *Kovove Mater.*, 2015 (in press)
34. ChVA Narasayya, P. Rambabu, M.K. Mohan, R. Mitra, and N.E. Prasad, Tensile Deformation and Fracture Behaviour of an Aerospace Aluminium Alloy AA2219 in Different Ageing Conditions, *Proc. Mater. Sci.*, 2014, **6**, p 322–330